Optical Materials 154 (2024) 115732

Contents lists available at ScienceDirect

Optical Materials

journal homepage: www.elsevier.com/locate/optmat

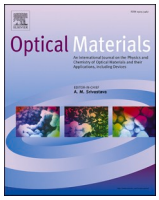

Research Article

Room-temperature tuning of mid-infrared optical phonons and plasmons in W-doped VO_2 thin films

Alessandro Bile [a], Daniele Ceneda [a], Vaghefi Esfidani S. Maryam [b], Daniele Scirè [c], Gianpiero Buscarino [d], Mauro Mosca [c], Dominique Persano Adorno [d], Roberto Macaluso [c], Roberto Li Voti [a], Concita Sibilia [a], Thomas G. Folland [b], Koray Aydin [e], Marco Centini [a], Maria Cristina Larciprete [a,*]

[a] Dipartimento di Scienze di Base ed Applicate per l'Ingegneria, Sapienza Università di Roma, Rome, 00161, Italy
[b] Department of Physics and Astronomy, University of Iowa, Iowa City IA, 52242 United States
[c] Department of Engineering, University of Palermo, Palermo, 90128, Italy
[d] Department of Physics and Chemistry "E. Segrè", University of Palermo, Palermo, 90128, Italy
[e] Department of Electrical and Computer Engineering, Northwestern University, Evanston IL 60208, United States

ARTICLE INFO

Keywords:
Phonon resonance tuning
Mid-IR photonics
Vanadium dioxide
Pulsed laser deposition
Phase-change materials
Thermochromics

ABSTRACT

The development of mid-infrared nanophotonics relies on the availability of new materials combining metal- and insulator-like optical features. We systematically studied the phase transition of thermochromic vanadium dioxide (VO_2) using substitutional tungsten doping at room temperature. Our results reveal that vanadium dioxide thin films, doped with tungsten and grown via pulsed laser deposition techniques on sapphire substrates, can be precisely engineered to exhibit tailored infrared phonon and plasmon polaritonic responses. By controlling the extent of tungsten concentration, starting from VO_2-WO_3 cold-pressed powder targets, we demonstrate the ability to continuously adjust both the amplitude and frequency of optical phonon resonances. Furthermore, we observe tunable free-electron response due to varying tungsten concentrations. The adopted fabrication technique makes it possible to create multilayer structures by alternating layers with different concentrations of tungsten. Our results pave the way for the development of tunable mid-infrared metamaterial devices operating at room-temperature.

1. Introduction

The interaction between electromagnetic radiation and materials in the mid-infrared(IR) can be influenced by either the response of free electrons or lattice ions, or a combination of both. In mid-IR wavelengths, low plasma frequency materials such as graphene [1], ITO [2], and 2D systems are specifically designed to tune the free-electron response [3] to excite and control surface plasmon polaritons (SPPs). Conversely, strong coupling of electromagnetic fields with lattice vibrations in polar materials enable the excitation of phonon polaritons and surface waves (SW) named surface phonon polaritons (SPhPs) [4].

The hybridization of transverse phonon polaritons with longitudinal optical phonons has the potential to develop efficient phonon polariton-based mid-infrared emitters [5–7]. Another form of SW hybridization can be achieved through plasmon-phonon coupling. Previous works have described graphene-based systems, where the excitation of hybrid plasmonic/phononic states is achieved through simultaneous excitation of plasmon modes in graphene and phonons in polar substrates such as SiC or HfO [8]. Similarly, graphene/h-BN heterostructures where surface plasmons of graphene couple with phonon polaritons of h-BN were investigated [9]. Moreover, doping-induced topological transitions by plasmon-phonon hybridization have been reported in graphene/α-MoO_3 heterostructures [10].

In the quest to realize tunable plasmonic and phononic responses, the optoelectronic properties of various materials are modulated by electron–phonon interactions. GaAs has been widely investigated since the seventies [11] to date [12]. Plasmon–phonon coupling in β-Ga_2O_3 has been shown to enhance the electron mobility by harnessing the dynamic screening of the electron–phonon interactions [13]. More recently, it was predicted that hybridized surface plasmon–phonon modes can be

* Corresponding author.
E-mail address: mariacristina.larciprete@uniroma1.it (M.C. Larciprete).

https://doi.org/10.1016/j.optmat.2024.115732
Received 7 April 2024; Received in revised form 20 June 2024; Accepted 23 June 2024
Available online 25 June 2024

observed in MoS_2 monolayer or even at the interface between MoS_2 and SiO_2 substrate [14].

This study focuses on vanadium dioxide (VO_2), a phase-transition material that undergoes metal-insulator transition (MIT) at a relatively low temperature [15]. Specifically, for temperatures below ~68 °C, VO_2 lattice displays a monoclinic phase characterized by an insulating state. Above the critical temperature, the crystal undergoes a structural phase transition to a tetragonal, (rutile) phase with metallic behavior. This phase transition results in drastic changes in electrical, optical, and thermal properties, making VO_2 attractive for applications such as smart infrared-emitters [16], optical modulators and filters [17,18]. More recently, photonics has opened to investigation and realization of neuromorphic circuits, exploiting materials able to modify themselves to emulate brain memory [19,20]. Within this context, VO_2 offers the possibility of saving different states as a function of temperature [21]. More importantly, the two different lattices, i.e. the extreme states of the phase-transition, support phononic and plasmonic response, respectively, in the same material although under different temperature conditions.

By doping VO_2 films with tungsten, it is possible to decrease the phase transition temperature, allowing the metallic phase to emerge at room temperature [22]. This feature has been intensively studied and employed for smart windows applications [23]. While doping is typically employed to modify electronic conduction properties in semiconductors, it also significantly alters the static and dynamic properties of the host material at the microscopic level [24]. Previous studies demonstrated how substitutional doping with tungsten modifies the electronic properties and the lattice dynamics of vanadium dioxide [25]. Specifically, the distortion introduced by W doping within the lattice structure supports the stabilization of the metallic phase with respect to the semiconducting phase [26,27], as sketched in Fig. 1. Therefore, it is possible to observe the metallic phase at room temperature [28,29].

In this work, we investigate a series of vanadium dioxide films with varying amounts of tungsten concentration, deposited on sapphire substrates using the pulsed laser deposition (PLD) technique. W-doped VO_2 films have been obtained from targets made of VO_2-WO_3 cold-pressed powders with different amounts of WO_3. Optical characterization has been performed at room temperature in the Mid-infrared range. Reflectance spectra, measured via FTIR highlight the effect of tungsten content on the infrared response of W-doped-VO_2 thin films evidencing an increasing plasmonic response due to free electrons for increasing W concentrations. Raman measurements confirm that the optical phonon response, intrinsic of the semiconducting VO_2 monoclinic phase weakens with increasing W-doping content favoring a more symmetric (with no Raman active phonons) rutile structure. We observe a complete transition from insulator to metal at room temperature in a VO_2 film with 5 % W concentration. Experimental results demonstrate the unique ability to tune and balance both phononic and plasmonic contributions within the same material by selecting the appropriate W concentration. Additionally, this technique allows the use of multiple targets with different W concentrations in the deposition chamber to fabricate thermochromic metallo/dielectric multilayer structures. Our results position W-doped VO_2 as a compelling material platform for tunable and dynamic mid-infrared applications such as thermal emitters, detectors, sensors among many others.

2. Results and discussion

VO_2 films with different amount of tungsten were deposited onto sapphire substrates by pulsed laser deposition technique (PLD) [30,31] using cold-pressed VO_2 powders with different amount of W concentration (namely, from 0 to 10 %). PLD deposition conditions (described in the fabrication methods) were the same for all samples.

Raman spectra of each investigated sample were performed to highlight the optical phonon response of VO_2 as function of W doping. The results are collected at room temperature using a Renishaw InVia microraman system with 514 nm excitation. Measured spectra are shown in Fig. 2. The Raman spectra are compared to the Sapphire substrate in Fig. S1 of the supporting information. For low W concentrations, the main Raman active phonon resonances of the monoclinic phase of VO_2 [29,32] are clearly visible. In particular, the strongest phonon mode at 615 cm^{-1} corresponds to a V–O mode which mainly involves the oxygen ions connecting the different V chains along the c-axis [32,33]. Its resonance frequency is slightly affected by doping, shifting from 615 to 620 cm^{-1}, however, its intensity is strongly dependent on the doping content. The emerging broadband signal with increasing W concentrations, is a signature of the electronic continuum background, superimposed to the phonon-modes. We also note that the Raman peak vanishes for a W concentration of 5 %. The observed decrease in the intensities of the Raman active modes and broadening of the peaks with an increase in the percentage of W doping can be explained by the fact that W doping starts to favor a more symmetric rutile structure. By group theory analysis, the monoclinic (insulator) phase is characterized by 18 Raman-allowed modes, 9 with A_g symmetry and 9 with B_g symmetry while the rutile (metallic) phase is characterized by a broad featureless luminescence [29].

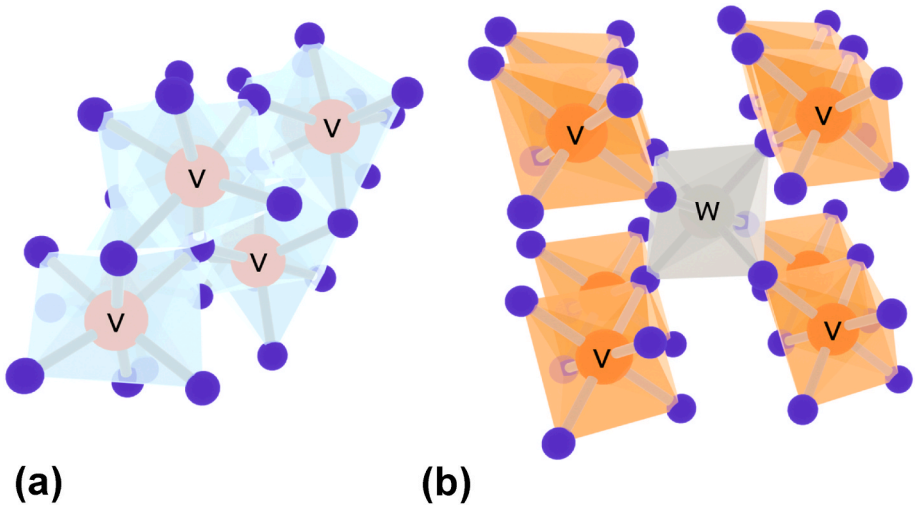

Fig. 1. Sketch of the VO_2 lattice structure in the (a) undoped, monoclinic insulating phase (below phase transition temperature), (b) tungsten-doped lattice, moving forward the tetragonal metallic phase (above phase transition temperature). Different atoms are represented by colored circles: large and orange for vanadium, small and purple for oxygen and, finally, large and grey represents tungsten in substitutional position.

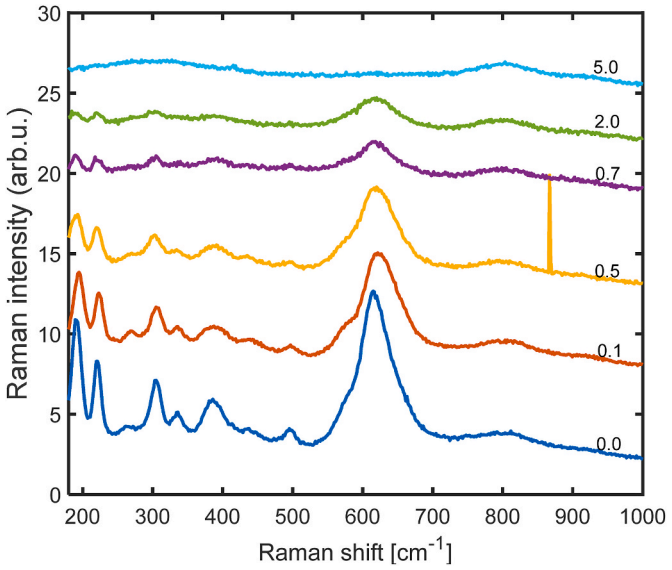

Fig. 2. Raman spectra of VO_2 films with varying W incorporation from 0.0 at% to 5.0 at%.

The surface morphology of undoped and W-doped VO_2 thin films was assessed by atomic force microscopy (AFM). AFM images reported in Fig. 3 show that all films are compact and uniform, and exhibit a very fine granularity. According to image software analysis, samples having a W-content up to 2 % exhibits a larger regularity with an average roughness of about 1.1 nm. On the other hand, increasing W-content up to 5 % and 10 % results in a gradual morphology change along with a significant increase in roughness (2.5–2.7 nm).

Furthermore, FT-IR spectra were measured in reflection mode, to highlight how doping level affects the infrared spectral features. We used a Bruker Invenio-R FT-IR spectrometer operating in 64-scan mode per measurement in the spectral range 1.5–25 μm and equipped with a glow-bar as radiation source. Reflectance was measured at 15° incidence angle, using a linear wide range infrared polarizer and setting two different polarizations for the incoming light, corresponding to in-plane (p-) and normal polarization (s-). However, the experimental findings displayed similar signals for measurements taken with s-polarization and p-polarization at nearly normal incidence (15°), thus indicating that the investigated films do not possess any optical anisotropy within the surface plane. Fig. S2 of the supporting information shows that, besides the small geometrical anisotropy introduced by the non-normal incidence angle (15°) s- and p-polarized spectra are very similar with the exception of the out of plane anisotropy of the Al_2O_3 substrate, clearly visible at 900 cm^{-1}. In order to simplify data analysis and fit of experimental spectra we focused our attention on s-polarized reflectance. Fig. 4 a-c reports s-polarized reflectance spectra recorded at room temperature for three samples corresponding to pure, 1 % W- and 5 % W- concentrations (blue curves).

We notice that the film response becomes metallic for 5 % W concentration while differences between pure and 1 % doped samples reveal an interplay between phononic and free electrons response. For completeness, we report the reflectance spectra for 0.1 %, 0.5 % 0.7 %, and 2 % W concentration layers in Fig. S3 of the supporting information. Each reflectance spectrum has been fitted by using a 4 × 4 transfer matrix method detailed in Ref. [34]. The adopted numerical method is widely used for anisotropic materials in ellipsometry setups. Indeed, it allows the calculation of the four complex reflection coefficients for layered structures, namely r_{ss}, r_{pp}, r_{sp} and r_{ps}, where ss (pp) stand for s-(p-) polarization of detected field and s-(p-) polarization for incident field respectively. The reflected field is written as a decomposition of s-

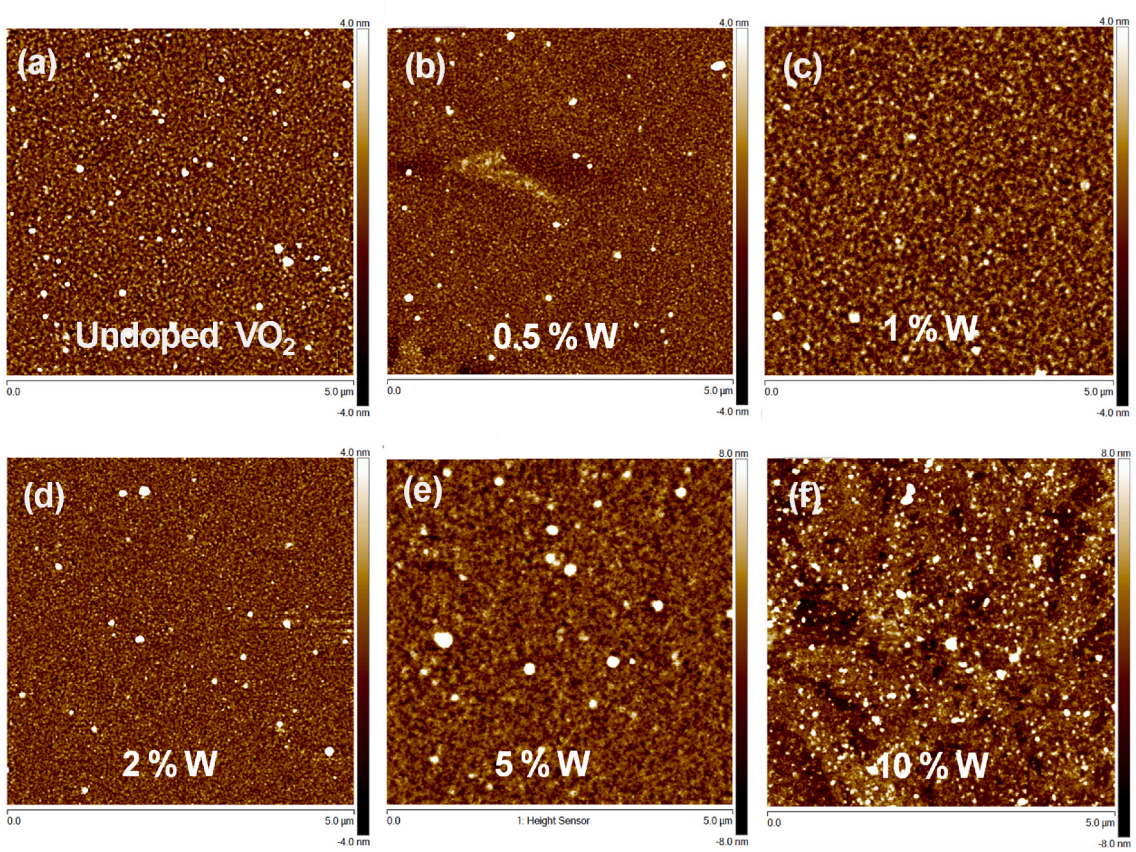

Fig. 3. AFM images of undoped (a), and W-doped (b–f) VO_2 thin films.

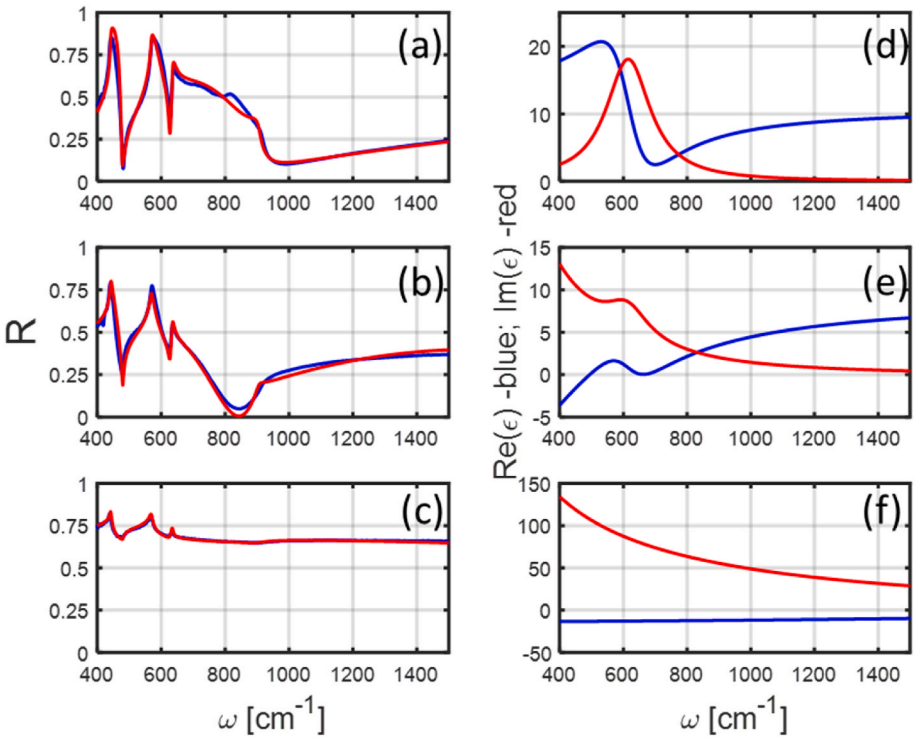

Fig. 4. Experimental (blue) and calculated (red) reflectance spectra of W-doped VO_2 films with different W concentrations: a) 0 %; b) 1 %; c) 5 %. Retrieved values of real (blue) and imaginary part of the dielectric function for d) 0 %, e) 1 %, f) 5 % W concentrations.

and p-polarized field:

$$E_s = r_{ss}\cos(\phi_{in}) + r_{sp}\sin(\phi_{in}) \quad (1a)$$

$$E_p = r_{pp}\sin(\phi_{in}) + r_{ps}\cos(\phi_{in}) \quad (1b)$$

where ϕ_{in} is the polarization angle of the incident field being: ϕ_{in} = 0 (90) s-pol (p-pol).

Due to the polycrystalline nature of the investigated films we used isotropic models for W-doped VO_2 films while the Al_2O_3 substrates display out of plane anisotropy. We note that all the cross-polarized reflection coefficients are zero in our case because there is no in-plane anisotropy. Thus, for our purposes we focused on the calculated s-polarized ($\phi_{in} = 0$) reflectance $R = |r_{ss}|^2$. Theoretical reflectance has been evaluated as a function of the thickness of the W-doped VO_2 films on top al Al_2O_3 semi-infinite substrates by proper modelling the electric permittivity of W-doped VO_2 films in the frequency range from 400 to 1500 cm^{-1}. More specifically the electric permittivity was modelled starting from a single Lorentz oscillator model corresponding to the main optical phonon mode around 620 cm^{-1} (extracted from the Raman spectra) and a Drude-like model to take account for the free electrons' contribution. All the other effects out of the 400-1500 cm^{-1} frequency range are included in the ε_∞ value. Thus, the adopted formula to model the electric permittivity is:

$$\varepsilon(\omega) = \varepsilon_\infty + \frac{S\omega_{TO}^2}{\omega_{TO}^2 - \omega^2 - i\gamma_{ph}\omega} - \frac{\omega_p^2}{\omega^2 + i\gamma_0\omega} \quad (2)$$

Where S is the phonon oscillator strength, ω_{TO} is the optical phonon resonance frequency extracted from Raman spectra, γ_{ph} is the damping of the phonon oscillator, ω_p is the plasma frequency corresponding to the free electron response and γ_0 is the damping factor related to ohmic losses. Experimental reflectance spectra have been fitted by considering all the six parameters of Eq [2]. The thickness of the VO_2 film is also assumed as a fit parameter. A least square method has been implemented to find the best-fit parameters comparing the experimental reflectance to the theoretically modelled one. Fitting curves for each sample are reported in Fig. 3 a-c (red line) and in Fig. S3. Retrieved fitting parameters for different films with different W- concentrations are reported in Table 1.

We note that the strength of the phonon oscillator becomes lower as the W concentration increases. This is confirmed by analysing the dielectric function retrieved from the fit parameters using Eq [1]. Fig. 4d–f depict the real and imaginary part of the dielectric function for (4d) pure VO_2 sample; (4e) 1 % W-doped VO_2 sample; (4f) 5 % W-doped VO_2 sample. The transition from dielectric to metal behaviour is clearly visible from the sign of the real part of the dielectric function going from positive to negative. The 1 % doped sample exhibits an intermediate condition, a weakened phonon response and an arising metal behaviour. At the same time the plasma frequency for the free electrons in the Drude model response grows from 300 cm^{-1} (insulator state of pure VO_2) to 12597 cm^{-1} (corresponding to a wavelength $\lambda = 794$ nm) according to the typical metallic behaviour observed. Finally, we compare the reflectance spectra for 2 % and 5 % W-doping samples: we note that the reflectance for the 2 % doped sample exhibits a decreasing slope vs frequency with respect to the 5 % sample reflectance. This effect is consistent with the smaller plasma frequency related to the free electrons response of 2 % doped sample making the electron screening effect less efficient at higher frequencies.

3. Conclusions

In conclusion, we have shown that tungsten-doped vanadium dioxide thin films can be fabricated with tailored optical infrared phononic and plasmonic response at room temperature by controlling the amount of tungsten doping. More in detail, our results show that it is possible to control the plasma frequency of the metallic response and the strength of the phonon resonance ranging from a pure insulator behaviour to a typical metallic response. The possibility to tame and tune both phononic and plasmonic frequencies makes doped VO_2 a unique appealing material for mid infrared applications. These findings have the potential

Table 1
Values of the fitting parameters retrieved from the reflectance spectra of different W-VO_2 films on sapphire substrate with varying W- incorporation. Modelled reflection spectra obtained with these parameters are plotted in Fig. 3 and Fig. S3. The last column reports the coefficient of determination for each modelled curve.

W-doping [%]	ε_∞	ω_p [cm^{-1}]	γ_0 [cm^{-1}]	ω_{TO} [cm^{-1}]	S	γ_{ph} [cm^{-1}]	Thickness [nm]	R^2
0	10.5	278	252	621	4.87	169	174	0.97
0.1	9.69	508	190	621	3.72	172	192	0.96
0.5	9.40	2015	397	615	1.65	174	391	0.98
0.7	8.95	1817	339	618	2.07	182	618	0.95
1	8.61	2010	363	618	1.05	165	641	0.97
2	5.88	6272	721	620	0.48	99	384	0.96
5	5.22	12597	2900	–	0	–	278	0.98

to surpass the limitations of plasmonics in terms of wavelength, leading to the development of tunable and integrated infrared (IR) devices. This advancement opens possibilities for several applications, including modulators, advanced sensors, thermal radiation control, tunable radiative cooling and all-optical neuromorphic applications.

4. Methods

4.1. Fabrication

All W-doped VO_2 films were deposited by PLD on sapphire substrate at 550 °C and 10^{-2} mbar oxygen pressure. Specific targets with different W atomic concentrations, namely 0 % (i.e., pure VO_2), 0.1 %, 0.5 %, 0.75 %, 1 %, 2 %, 5 %, and 10 % were prepared by cold pressing VO_2 and WO_3 powders together. The PLD process was carried out by employing a Q-switched Nd:YAG laser with a pulse width of 6 ns and a repetition rate of 4 Hz [24,26].

4.2. Raman measurements

To study vibrational modes of W-doped VO_2 films, Raman spectra are obtained at the room temperature in the air environment. The measurement is conducted using a Renishaw inVia Raman Microscope system in a backscattering configuration, with an incident wavelength of 514 nm of Argon laser focused through an 20× objective with NA of 0.4, a 1200I/mm grating and the laser spot size of approximately 2 μm. Each point is exposed for the duration of 10s to ensure accurate data accusation. A total of 10 sample scans are collected with an accumulation time of 10s for cosmic ray removal.

4.3. Atomic force microscopy (AFM)

Films' morphology was assessed by using a Bruker FAST-SCAN atomic force microscope. Measurements were performed in air with the microscope working in soft tapping mode using a FAST SCAN A probe having triangular shape, nominal tip radius of 5 nm and nominal spring constant of 17 N/m. The tip velocity on the surface and the PID gains were optimized to give the higher scan rate compatibly with a reliable scan of the surface. The optimal tip velocity was found to be 20 μm/s. The scan size was fixed at a value of 5 μm × 5 μm. Each AFM image has a pixel resolution (lateral resolution) comparable to the tip size.

4.4. FTIR spectroscopy

IR reflectance measurements were performed using an FT-IR interferometer (Invenio-R, Bruker) in the spectral range of 7–25 μm. We use a glow-bar as the IR source and deuterated triglycine sulfate (DTGS) pyroelectric element as the IR detector. A total number of 64 interferograms were acquired for each measurement, with a spectral resolution of 2 cm^{-1}. Knife edge apertures were set to 3 × 3 mm^2 to select a defined sample area during IR data acquisition. The FT-IR platform is equipped with a reflectance unit allowing to select the angles of incidence and reflectance, which was set to 15°. The polarization state of incident light can be selected using a wide-range holographic polarizing filter with a motorized mounter. Before each measurement run, the reflectance spectra were recorded at both room temperature and at about 100 °C so that the phase transition of VO_2 is completed using two different, crossed, linear polarization states of the incoming light.

CRediT authorship contribution statement

Alessandro Bile: Writing – original draft, Software, Investigation, Formal analysis, Data curation. **Daniele Ceneda:** Software, Investigation, Formal analysis. **Vaghefi Esfidani S. Maryam:** Visualization, Methodology, Investigation, Data curation. **Daniele Scirè:** Resources, Investigation, Data curation. **Gianpiero Buscarino:** Investigation. **Mauro Mosca:** Resources, Investigation, Data curation. **Dominique Persano Adorno:** Resources, Investigation, Data curation. **Roberto Macaluso:** Writing – original draft, Visualization, Resources, Methodology, Investigation. **Roberto Li Voti:** Validation, Investigation, Formal analysis, Data curation. **Concita Sibilia:** Visualization, Validation, Supervision, Methodology, Investigation. **Thomas G. Folland:** Writing – review & editing, Visualization, Validation, Investigation, Formal analysis, Data curation. **Koray Aydin:** Writing – review & editing, Validation, Supervision, Investigation, Funding acquisition, Formal analysis. **Marco Centini:** Writing – review & editing, Writing – original draft, Validation, Supervision, Methodology, Investigation, Formal analysis, Conceptualization. **Maria Cristina Larciprete:** Writing – original draft, Supervision, Methodology, Investigation, Funding acquisition, Conceptualization.

Declaration of competing interest

The authors declare that they have no known competing financial interests or personal relationships that could have appeared to influence the work reported in this paper.

Data availability

Data will be made available on request.

Acknowledgments

K.A. and M.C.L. acknowledge Accordi Bilaterali Interuniversitari 2022 program from Sapienza University (Prot. AI2620PAR2, Bando Professori Visitatori 2022). K.A. acknowledges partial support from the Air Force Office of Scientific Research under award number FA9550-22-1-0300. The work was financed by the European Union—NextGenerationEU (Bando PRIN 2022, Directorial Decree n. 104—February 02, 2022, Project code: 2022ZRN4LX). The opinions expressed are those of the authors only and should not be considered representative of the European Union or the European Commission's official position. Neither the European Union nor the European Commission can be held responsible for them.

Appendix A. Supplementary data

Supplementary data to this article can be found online at https://doi.org/10.1016/j.optmat.2024.115732.

References

[1] A. Grigorenko, M. Polini, K. Novoselov, Graphene plasmonics, Nature Photon 6 (2012) 749–758.
[2] S. Franzen, C. Rhodes, M. Cerruti, R.W. Gerber, M. Losego, J.-P. Maria, D. E. Aspnes, Plasmonic phenomena in indium tin oxide and ITO-Au hybrid films, Opt. Lett. 34 (2009) 2867–2869.
[3] L.Z. Liu, K. Aydin, Enhanced infrared transmission through gold nanoslit arrays via surface plasmons in continuous graphene, Opt Express 24 (2016) 27882–27889.
[4] J.D. Caldwell, L. Lindsay, V. Giannini, I. Vurgaftman, T.L. Reinecke, S.A. Maier, O. J. Glembocki, Low-loss, infrared and terahertz nanophotonics using surface phonon polaritons, Nanophotonics 4 (2015) 44–68.
[5] G. Lu, C.R. Gubbin, J.R. Nolen, T. Folland, M.J. Tadjer, S. De Liberato, J. D. Caldwell, Engineering the spectral and Spatial Dispersion of thermal emission via Polariton−Phonon strong coupling, Nano Lett. 21 (4) (2021) 1831–1838.
[6] C.R. Gubbin, R. Berte, M.A. Meeker, A.J. Giles, C.T. Ellis, J.G. Tischler, V. D. Wheeler, S.A. Maier, J.D. Caldwell, S. De Liberato, Hybrid longitudinal-transverse phonon polaritons, Nat. Commun. 10 (1) (2010) 1682.
[7] M.C. Larciprete, S. Abedini Dereshgi, M. Centini, K. Aydin, Tuning and hybridization of surface phonon polaritons in α-MoO_3 based metamaterials, Opt Express 30 (2022) 12788–12796.
[8] E.H. Hwang, Rajdeep Sensarma, S. Das Sarma, Plasmon-phonon coupling in graphene, Phys. Rev. B 82 (2010) 195406.
[9] I.D. Barcelos, A.R. Cadore, L.C. Campos, A. Malachias, K. Watanabe, T. Taniguchi, F.C.B. Maia, R. Freitasd, C. Deneke, Graphene/h-BN plasmon–phonon coupling and plasmon delocalization observed by infrared nano-spectroscopy, Nanoscale 7 (2015) 11620–11625.
[10] F.L. Ruta, B.S.Y. Kim, Z. Sun, D.J. Rizzo, A.S. McLeod, A. Rajendran, A.J. Millis, J. C. Hone, D.N. Basov, Surface plasmons induce topological transition in graphene/α-MoO_3 heterostructures, Nat. Commun. 13 (2022) 3719.
[11] A.A. Kukharskii, Plasmon-phonon coupling in GaAs, Solid State Commun. 13 (1973) 1761–1765.
[12] W. Streyer, K. Feng, Y. Zhong, A. Hoffmann, D. Wasserman, Engineering the Reststrahlen band with hybrid plasmon/phonon excitations, MRS Communications 6 (2016) 1–8.
[13] A. Kumar Rajapitamahuni, A. Kamath Manjeshwar, A. Kumar, A. Datta, P. Ranga, L. Raju Thoutam, S. Krishnamoorthy, U. Singisetti, B. Jalan, Plasmon–phonon coupling in electrostatically gated β-Ga_2O_3 films with mobility exceeding 200 $cm_2 V^{-1} s^{-1}$, ACS Nano 16 (6) (2022) 8812–8819.
[14] H.M. Dong, Z.H. Tao, Y.F. Duan, F. Huang, C.X. Zhao, Coupled plasmon-phonon modes in monolayer MoS_2, J. Phys. Condens. Matter 32 (12) (2019) 125703.
[15] A. Zylbersztejn, N.F. Mott, Metal-insulator transition in vanadium dioxide, Phys. Rev. B 11 (1975) 4383–4396.
[16] M.C. Larciprete, M. Centini, S. Paoloni, I. Fratoddi, S.A. Dereshgi, K. Tang, J. Wu, K. Aydin, Adaptive tuning of infrared emission using VO_2 thin films, Sci. Rep. 10 (2020) 11544.
[17] M.T. Nouman, J. Hyun Hwang, M. Faiyaz, K.J. Lee, D.Y. Noh, J.-H. Jang, Vanadium dioxide based frequency tunable metasurface filters for realizing reconfigurable terahertz optical phase and polarization control, Opt Express 26 (2018) 12922–12929.
[18] S. Abedini Dereshgi, M.C. Larciprete, M. Centini, A.A. Murthy, K. Tang, J. Wu, V. P. Dravid, K. Aydin, Tuning of optical phonons in α-MoO_3-VO_2 Multilayers, ACS Appl. Mater. Interfaces 13 (41) (2021) 48981–48987.
[19] H. Tari, A. Bile, F. Moratti, E. Fazio, Sigmoid type neuromorphic activation function based on saturable absorption of graphene/PMMA composite for intensity modulation of surface plasmon polariton signals, Plasmonics 17 (2022) 1025–1032.
[20] A. Bile, M. Chauvet, H. Tari, E. Fazio, Supervised learning of soliton X-junctions in lithium niobate films on insulator, Opt. Lett. 47 (2022) 5893–5896.
[21] S. Carapezzi, C. Delacour, A. Plews, A. Nejim, S. Karg, A. Todri-Sanial, Role of ambient temperature in modulation of behavior of vanadium dioxide volatile memristors and oscillators for neuromorphic applications, Sci. Rep. 12 (2022) 19377–19386.
[22] Y. Bleu, F. Bourquard, V. Barnier, A.-S. Loir, F. Garrelie, C. Donnet, Towards room temperature phase transition of W-doped VO_2 thin films deposited by pulsed laser deposition: thermochromic, surface, and structural analysis, Materials 16 (2023) 461.
[23] Z. Huang, C. Chen, C.L.S. Chen, Tungsten-doped vanadium dioxide thin films on borosilicate glass for smart window application, J. Alloys Compd. 564 (2013) 158–161.
[24] S. Wall, D. Wegkamp, L. Foglia, K. Appavoo, J. Nag, R.F. Haglund, J. Staehler, M. Wolf, Ultrafast changes in lattice symmetry probed by coherent phonons, Nat. Commun. 3 (2012) 721–727.
[25] K. Appavoo, J. Nag, B. Wang, W. Luo G. Duscher, E.A. Payzant, et al., Doping-driven electronic and lattice dynamics in the phase-change material vanadium dioxide, Phys. Rev. B 102 (2020) 115148–115158.
[26] X. Tan, T. Yao, R. Long, Z. Sun, Y. Feng, H. Cheng, X. Yuan, et al., Unraveling metal-insulator transition mechanism of VO_2 triggered by tungsten doping, Sci. Rep. 2 (2012) 466.
[27] G. Pan, J. Yin, K. Ji, X. Li, X. Cheng, H. Jin, J. Liu, Synthesis and thermochromic property studies on W doped VO_2 films fabricated by sol-gel method, Sci. Rep. 7 (2017) 6132.
[28] M.C. Larciprete, D. Ceneda, D. Scirè, M. Mosca, D.P. Adorno, S. Abedini Dereshgi, R. Macaluso, R. Li Voti, C. Sibilia, T. Cesca, G. Mattei, K. Aydin, M. Centini, Tunable IR perfect absorbers enabled by tungsten doped VO_2 thin films, Apl. Mater. 11 (9) (2013) 091107.
[29] L. Whittaker, T.L. Wu, A. Stabile, G. Sambandamurthy, S. Banerjee, Single-nanowire Raman microprobe studies of doping-, temperature-, and voltage-induced metal-insulator transitions of $W_{(x)}V_{(1-x)}O_2$ nanowires, ACS Nano 22 (5) (2011) 8861–8867, 11.
[30] H.U. Krebs, M. Weisheit, J. Faupel, E. Süske, T. Scharf, C. Fuhse, M. Störmer, K. Sturm, M. Seibt, H. Kijewski, D. Nelke, E. Panchencko, M. Buback, Pulsed laser deposition (PLD) – A versatile thin film technique, Adv. Solid State Phys. 43 (2003) 505–518.
[31] A. Boughelout, R. Macaluso, I. Crupi, B. Megna, A. Brighet, M. Trari, M. Kechouane, Effect of the Si doping on the properties of AZO/SiC/Si heterojunctions grown by low temperature pulsed laser deposition, Semicond. Sci. Technol. 36 (2021) 15001–150012.
[32] C. Marini, E. Arcangeletti, D. Di Castro, L. Baldassare, A. Perucchi, S. Lupi, L. Malavasi, L. Boeri, E. Pomjakushina, K. Conder, P. Postorino, Optical properties of $V_{1-x}Cr_xO_2$ compounds under high pressure, Phys. Rev. B 77 (2008) 235111.
[33] P. Schilbe, Raman scattering in VO_2, Phys. B Condens. Matter 316–317 (2002) 600–602.
[34] N.C. Passler, A. Paarmann, Generalized 4× 4 matrix formalism for light propagation in anisotropic stratified media: study of surface phonon polaritons in polar dielectric heterostructures, JOSA B 34 (10) (2017) 2128–2139.